Ultrafast Excited and Ground-State Dynamics of the Green Fluorescent Protein Chromophore in Solution

Mikas Vengris,[†] Ivo H. M. van Stokkum,[†] Xiang He,[‡] Alasdair F. Bell,[‡] Peter J. Tonge,[‡] Rienk van Grondelle,[†] and Delmar S. Larsen*,[†]

Faculty of Sciences, Vrije Universiteit Amsterdam, De Boelelaan 1081, 1081 HV Amsterdam, The Netherlands, and Department of Chemistry, State University of New York at Stony Brook, Stony Brook, New York 11794-3400

Received: December 17, 2003; In Final Form: February 26, 2004

Ultrafast dispersed pump-dump-probe spectroscopy was applied to HBDI (4′-hydroxybenzylidene-2,3-dimethyl-imidazolinone), a model green fluorescent protein (GFP) chromophore in solution with different protonation states. The measured three-dimensional data was analyzed using a global analysis method that enables the spectral and temporal characterization of overlapping photoinduced transient states. A unified phenomenological model is presented to describe the observed data. Two excitation pathways are identified: a 1-photon excited-state twisting and a 2-photon ionization process. The ionization pathway results in the generation of solvated electrons and HBDI radicals. The twisting dynamics was resolved on both electronic states with slower twisting on the ground state than the excited state. This is ascribed to the multidimensional hula-twist mechanism. A weak viscosity dependence was observed when the aqueous solution data were contrasted with the signals collected in a 66% glycerol/water solution.

1. Introduction

In recent years, the green fluorescent protein (GFP) first isolated from the jellyfish *Aequorea victoria* has become a widely used fluorescent probe in molecular biology.[1−3] In contrast to potentially toxic fluorescent dyes, GFP can be genetically attached to other proteins, enabling experimentalists to easily monitor their distribution and movement in cells.[4,5] GFP has the distinctive property of forming the intrinsic fluorescent chromophore autocatalytically out of a sequence of three amino acid residues (Ser65-Tyr66-Gly67). This further adds to the utility of GFP as a biological probe because the introduction of external cofactor molecules is not required for the development of its spectroscopic properties.[6]

The absorption spectrum of the GFP protein exhibits two resolvable bands, while its observed fluorescence spectrum has a single band. The constituent absorption bands at 395 and 475 nm have been ascribed to the neutral and anionic deprotonated states of the GFP chromophore, respectively, and the fluorescence is ascribed solely to the anionic form.[7−10] It is believed that upon excitation of the neutral chromophore, a rapid deprotonation reaction of the chromophore occurs where the proton is donated to a nearby water molecule within the protein pocket, resulting in a green fluorescence that is emitted by the anionic state of the chromophore.[8,11,12]

The observed photodynamics of the isolated GFP chromophore in solution (4′-hydroxybenzylidene-2,3-dimethyl-imidazolinone, HBDI) has strikingly different spectroscopic properties from the GFP protein.[13−15] Although the excited-state lifetime of GFP protein is 3.3 ns,[11] the isolated GFP chromophore is virtually nonfluorescent in room-temperature liquids with a ∼1 ps excited-state lifetime.[6,15−17] The popular explanation for this marked difference in these lifetimes is that the GFP protein scaffolding hinders the isomerization reaction about the bridging bond between the phenolic and imidazolinone rings in the chromophore (Figure 1). In the absence of the protein, the chromophore will undergo excited state twisting that enhances internal conversion and considerably shortens the fluorescence lifetime.[15,17−22] In HBDI, this quenching process depends weakly on solvent viscosity, although it exhibits a pronounced temperature dependence.[15,21] The hula-twist isomerization mechanism, involving rotational motion of two molecular bonds,[23,24] has been proposed as the main channel of excited-state decay.[14,25] The volume-conserving aspect of the hula-twist mechanism, was used to explain the weak viscosity dependence of the HBDI quenching time scales.[14]

To understand how the protein environment modulates the underlying dynamics of GFP, it is essential to understand the dynamics inherent to the chromophore. We have performed dispersed pump−dump−probe (PDP) experiments on the synthetic GFP model chromophore, HBDI, in aqueous solutions at different pHs and also in a 66% glycerol/water solution. These multi-pulse experiments are useful in the cases when the system exhibits complex light-induced dynamics involving multiple excited state evolution pathways with spectrally overlapping bands.[26−29] The PDP technique builds upon more traditional pump−probe (PP) techniques. First, an ultrafast pulse brings the sample into an excited state, after which, a second laser pulse that is resonant with the stimulated emission (SE) is applied which demotes the excited chromophores back to the ground electronic state. This allows for a greater spectroscopic insight into ground and excited-state potential surfaces, along which the molecule is evolving. On the basis of these experiments, a unified phenomenological scheme describing both the excited and ground-state dynamics of HBDI is proposed.

* To whom correspondence should be addressed. E-mail: dslarsen@nat.vu.nl. Phone: +31 (0)20 444-7426. Fax: +31 (0)20 444-7999.
[†] Vrije Universiteit Amsterdam.
[‡] State University of New York at Stony Brook.

10.1021/jp037902h CCC: $27.50
Published on Web 05/05/2004

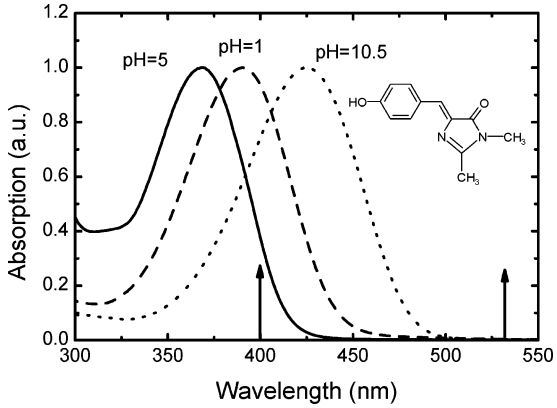

Figure 1. Absorption spectra of HBDI at different pH values. The arrows indicate the excitation and dump wavelength for ultrafast experiments. The inset shows the structural formula of HBDI at pH 5.

2. Materials and Methods

2.1. Experimental. The HBDI chromophore was synthesized according to the procedure described earlier.[16,30] For the experiments measured at pH 10.5 and 5, the sample was dissolved in 50 mM CAPS and 50 mM Tris buffers, respectively. For the pH 1 solution, the HBDI sample was dissolved in a 0.1 M HCl water solution instead. HBDI has two protonation sites: the phenolic oxygen ($pK_a = 8.2$) and the imidazolinone ring nitrogen ($pK_a = 1.8$).[30] Therefore, the three distinct protonation states exist and can be easily distinguished in aqueous solutions at different pHs by their absorption spectra (Figure 1). The anionic form (high pH), with an absorption maximum at 428 nm, is the form most similar to the fluorescent state of GFP,[7−10] whereas the neutral form, with a spectrum peaking at 368 nm, is most similar to the GFP state that is excited at 400 nm.[12] The low-pH cationic form does not have a known biological significance. A fourth zwitterionic state has been proposed to account for blinking phenomena in single molecule experiments;[25] however, no experimental evidence exists to support the existence of this state as a stable species.[30,31]

The pump−probe setup has been described in detail earlier and has been modified to include an additional pulse.[32,33] The basis of the system is a 1-kHz amplified Ti:sapphire system (BMI α) delivering 450-μJ, 60-fs, 800-nm pulses. The dispersed PDP experimental results presented here involve intense laser pulses at two wavelengths: 400 and 530 nm. The 400-nm pump pulses were generated by frequency-doubling a portion of the amplified 800-nm light in a 0.5 mm BBO crystal, whereas the 530-nm dump pulses were generated with a home-built noncollinear optical parametric amplifier pumped by the second harmonic of the 800-nm amplified light. The white-light continuum, used as the broad-band probe pulse, was produced by focusing a weak 800-nm beam into a slowly translating CaF_2 crystal. Reflective optics steered and focused the probe beam, reducing the group velocity dispersion to ~300 fs over 400−700 nm. The sample (OD ca. 0.6 at the absorption maximum) was pumped through a rapidly translating 1-mm quartz flow cell (rapid translation ensured that the sample was renewed between the consecutive laser pulses, and the flowing allowed to avoid the accumulation of any potential photoproducts). Two separate computer-directed translation stages controlled the time delays between the three pulses. The polarizations of the pump and dump pulses were kept parallel to each other and at magic angle (54.7°) to the probe pulse. Pump and dump pulse intensities of ca. 250 nJ/pulse were used. The pump and dump beam spot size at the focus were around 300 μm. The collected data have a wavelength resolution of 1 nm. An average noise level of <1 mOD was estimated. A 125 fs instrument response function, IRF, in the time domain was estimated from cross-phase modulation measurements on water. The dump probe data from this experiment were also used to provide an estimate for the group velocity dispersion of the probe, since only cross-phase modulation is observed uncluttered by the resonant signals. This estimate was further refined in the global fitting procedure to provide the best description of the data. All of the time-resolved data presented in this manuscript are dispersion corrected.

In practice, PDP data consists of three different data sets: (1) conventional pump−probe signal (PP), i.e., the situation when the pump pulse is on and the dump pulse is off; (2) pump−dump−probe signal (PDP), i.e., when both pump and dump pulses are on; (3) dump−probe signal (DP), i.e., when only the dump pulse is on. In our case, the dump pulse is not resonant with the ground-state absorption, however, any nonresonant coherent contributions which affect the spectra PDP can be subtracted, thus enabling scattering and cross-phase modulation artifacts to be removed. For visualizing the effect of the dump pulse, it is convenient to define a double difference absorption signal[33]

$$\Delta\Delta\mathrm{OD}(\lambda,t) = \mathrm{PDP}(\lambda,t) - \mathrm{PP}(\lambda,t) - \mathrm{DP}(\lambda,t) \qquad (1)$$

This signal represents the difference between pump−probe signals in the presence and absence of the dump pulse and is mostly free from the coherent artifacts from the dump pulse.

2.2. Data Analysis. The collected data were fitted using the global analysis technique described previously.[34,35] Underlying this analysis is the construction of a connectivity scheme, which describes how transient states are linked (e.g., in series, parallel, or an admixture of both). In the case of pump−dump−probe spectroscopy, the compartmental connectivity scheme results in the following set of differential equations

$$\frac{\mathrm{d}c_i}{\mathrm{d}t} = A_i I_{\mathrm{pump}}(t) + \sum_{j=1}^{N} K_{ij} c_j(t) + I_{\mathrm{dump}}(t - \tau_{\mathrm{dump}}) \sum_{j=1}^{N} B_{ij} c_j(t) \qquad (2)$$

where c_j is the time dependent concentration of the jth state. A_i is the coefficient, showing to which extent the pump pulse excites ith compartment; K_{ij} are the rates with which ith state is populated from the jth state; B_{ij} shows the efficiency with which jth compartment is dumped into the ith state. $I_{\mathrm{pump}}(t)$ and $I_{\mathrm{dump}}(t - \tau_{\mathrm{dump}})$ are the temporal responses (from the IRF) from the pump and dump pulses respectively; N is the total number of compartments used in the fitting. These differential equations are then solved to determine the time-dependent concentrations of the transient states in the case of pump-dump-probe data. The model function $F_{\mathrm{PDP}}(t,\lambda)$ used in the global analysis to fit the PDP(λ,t) data is then

$$F_{\mathrm{PDP}}(t,\lambda) = \sum_{i=1}^{N} \Delta\epsilon_i(\lambda) c_i(t) \qquad (3)$$

where $\Delta\epsilon_i(\lambda)$ is a the wavelength-dependent amplitude of the ith resulting concentration called the species-associated difference spectrum (SADS). The SADS and the coefficients A_{ij} and B_{ij} and rate constants K_{ij} are the free parameters of the fitting routine. For fitting the PP(λ,t) data, B_{ij} in eq 2 is set to zero.

The target analysis gives several important benefits. First, it allows the experimentalist to quantify the results in terms of microscopic rate constants K_{ij} and the SADS for different compartments. Second, it reduces the unwieldy set of PDP and PP data (both two-dimensional surfaces) into the smaller set of

spectra (SADS); in conjunction with the underlying connectivity scheme and the relatively small number of rate constants, this greatly simplifies the interpretations of our complex data.[34,35] The presence of the dump pulse provides additional information for the resolution of multiple transient state dynamics.

It is important to realize that this approach is phenomenological and its results should be interpreted with caution, just like interpreting more conventional single wavelength traces. Even though such analysis can be used to describe the measured data, not all phenomena exhibit underlying stepwise dynamics assumed by the system of differential equations outlined in eq 2 (e.g., solvation dynamics or underdamped vibrational wave packets). Thus, the discreet states in the connectivity scheme may not have to necessarily represent real electronic or vibronic states but rather stand for spectral forms with specific difference absorption spectra with specific temporal dependences. Hence, we adopt the term "excited (ground) state intermediates" to refer to such spectral forms. Neither does compartmental modeling imply that discreet exponential transition processes are taking place. However, processes involving a transition through a continuum of states, such as solvation or vibrational cooling, can be often described as a sum of exponentials.[33,36] Normally, the smallest possible number of states are introduced into the model that adequately describes the experimental data. Given a fixed number of compartments, more than one model will exist that will fit the data equally well.[28,37] The SADS in those cases will be linear combinations of the "real" SADS. The choice of the preferred model is based on the a priori knowledge about the shapes of the SADS and the intuition about the underlying physics of the connectivity scheme.

Since transient absorption experiments measure difference spectra, the corresponding SADS may have contributions from the ground-state bleach (GSB), stimulated emission (SE), and excited-state absorption (ESA), if the compartment represents an excited state. In the case of a ground-state compartment (e.g., photoproduct state or nonequilibrated ground species), only the GSB and the induced absorption will contribute to the resulting SADS. When the constituent transient states cannot be resolved unambiguously from the experimental data, the resulting SADS represent dynamics and spectra of a mixture of transient states.

A commonly used connectivity scheme is the sequential unidirectional model (e.g., state A $\rightarrow$ B $\rightarrow$ C etc.). In this case, the corresponding SADS represent the difference absorption spectra as a state "evolves" into the next state. Such an analysis establishes the time scales and the character of spectral evolution without necessarily ascribing physical meaning to each SADS. Alternatively, a parallel model can be used where different components decay independently from each other. Such a model is similar to the ubiquitous "sum of exponentials" fitting that is common in time-resolved spectroscopies. Often, the underlying connectivity schemes in ultrafast experiments are neither "parallel" nor "sequential" but involve a complicated combination of both. Such branched connectivity schemes have been successfully used to describe the ultrafast dynamics in many biological and physical studies.[38−40]

3. Results

3.1. Pump-Probe Data. Before delving into the PDP experiment or global analysis results, it is useful to extract some qualitative information and intuition from the raw (dispersion corrected) data directly. Representative PP traces and transient spectra for HBDI in water at pH 1, 5, and 10.5 and in 66% glycerol/water mixture at pH = 10.5 are displayed in Figure 2; three (four at pH 10.5) overlapping bands are distinguished in the measured spectra. The ground state bleach is observed as a negative band at the wavelengths corresponding to the absorption spectra (Figure 1), and the pronounced negative band to the red of the GSB (the wavelengths corresponding to HBDI fluorescence spectra) is ascribed to SE. The positive band observed between the GSB and SE bands at longer times is an induced absorption which exhibits a delayed appearance with respect to both the GSB and SE band (Figure 2A,C,E,G dashed curves) and also decays on a slightly slower time scale.

In the pH 10.5 samples, a second induced absorption band is observed to the blue ($<$375 nm) of the GSB (Figure 2B,D) which is not observed in the data collected at other pHs, most probably because it lies outside the spectral window of the detector. In contrast to the induced absorption band in the visible, the positive UV band in the pH 10.5 sample is generated instantly (in the glycerol sample, its rise is partially obscured by the cross-phase modulation artifact) and decays with the same time scale as the SE band (Figure 2A,C dotted curves). The dynamics measured at 350 nm is also distinctly different from the dynamics of the induced absorption at 470 nm (Figure 2A,C dashed curves), suggesting that these bands have different origins.

The PP signals in all three solutions exhibit similar spectral trends, but with differing kinetics. Normalized traces probed in the SE bands (525 nm) are contrasted in Figure 3 and a clear pH dependence is observed. Since the SE overlaps with the induced absorption of long-lived transient states, a terminal nonzero value is observed (vide infra); however, the difference in the picosecond decay kinetics is clearly distinguishable. The slowest time scale is observed in the viscous glycerol-containing sample (filled triangles) and is followed by the anionic HBDI sample at pH 10.5 (hollow diamonds) and then the cationic HBDI sample at pH 1 (filled squares). Furthermore, the chromophore in the neutral solution (hollow circles) decays considerably faster than the rest. Similar differences between anionic and neutral form of HBDI have been observed in the time-resolved fluorescence experiments.[13,21] The overlapping bands and dynamics suggest that a full global analysis is required to extract the time scales in these data.

The measured PP signals in all samples exhibit long-lived components that persist for the duration of the experimental window ($\sim$5 ns). These "terminal" spectra (Figure 2B,D,F,H dot−dashed curves) exhibit a GSB contribution together with two induced absorption bands that are appreciably different from those discussed above. The narrower ($\sim$40 nm fwhm) induced absorption band is resolved just to the red of GSB, in the same region as the visible induced absorption band, though with distinguishably different kinetic properties (vide supra). A second, broad ($>$100 nm fwhm) band that peaks further to the red than 650 nm is more noticeable as it seemingly extends across the larger part of the observed spectrum. At pH 10.5, the narrower band overlays the GSB and extends to the UV.

In the pH 1 sample, the terminal spectrum is not technically terminal and exhibits resolved decay dynamics (Figure 5). The broad induced absorption component of this spectrum exhibits a $\sim$400 ps decay (hollow circles). In sharp contrast, the GSB and narrow absorption band exhibit no noticeable evolution. The PP signals measured in the other solutions do not show such dynamics. This decay is described in terms of a scavenging effect from the excess protons in the low pH sample and will be touched on further in the Discussion.

The terminal spectrum was further explored with power-dependent PP signals. Figure 4 shows the excitation energy dependence of the difference absorption signal measured in

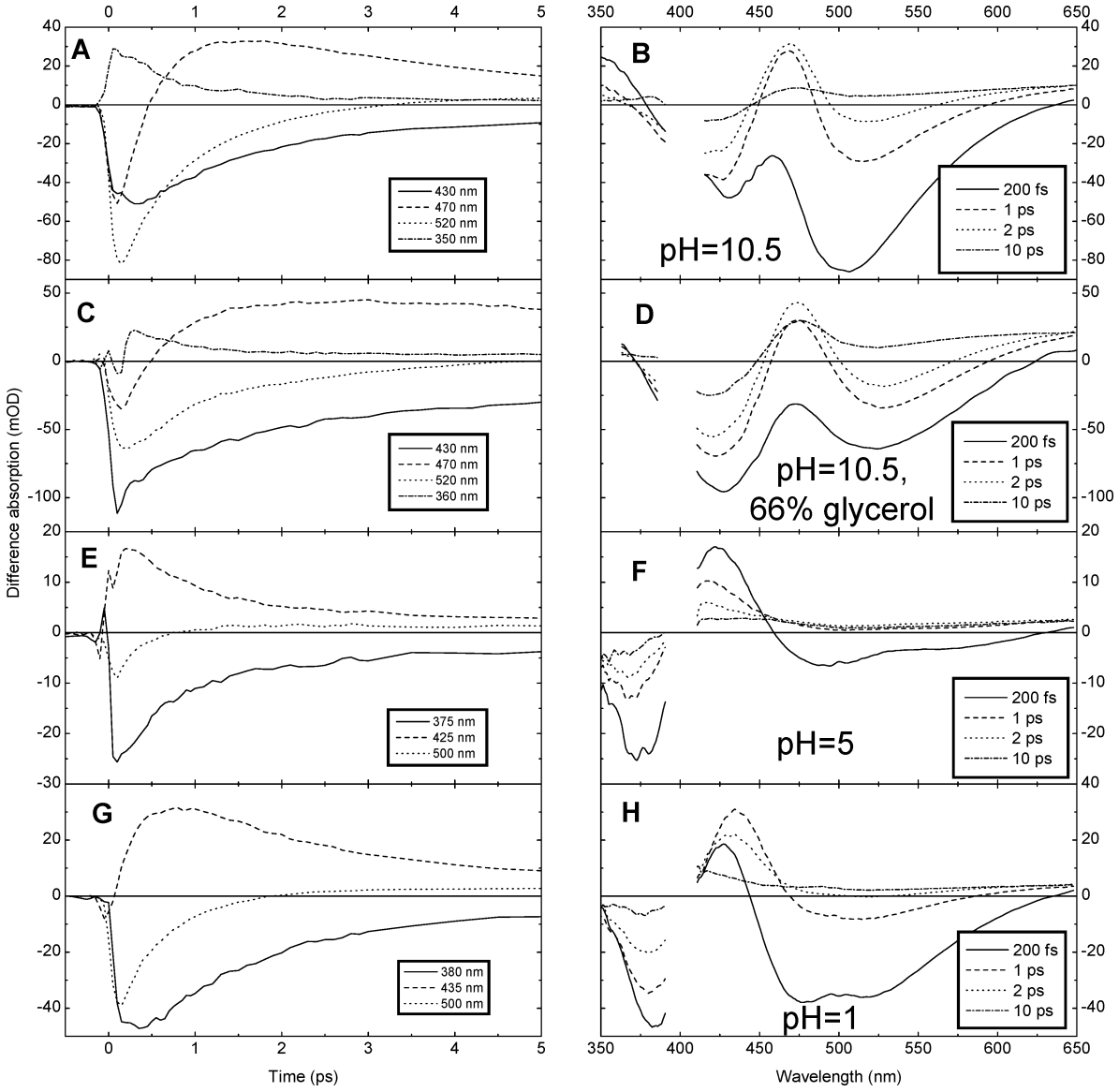

Figure 2. Left: pump−probe traces of HBDI in water at pH 10.5 (A), pH 5 (E), and pH 1 (G) and water−glycerol mixture (C). Right: time-gated pump−probe spectra measured at 200 fs (solid lines), 1 ps (dashed lines), 2 ps (dotted lines), and 10 ps (dash−dotted lines) after the excitation pulse. The data have been corrected for group velocity dispersion. The spectral region between 385 and 405 nm was affected by the scattering of the pump pulse and was removed from the original data.

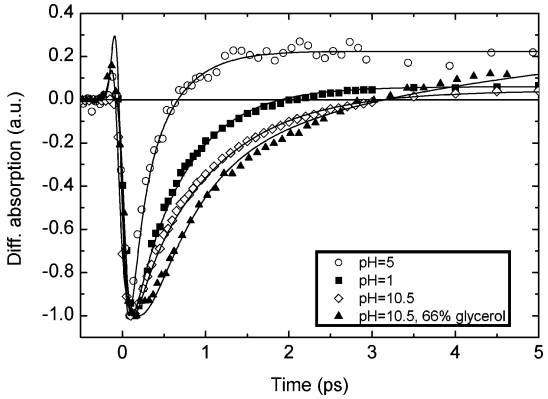

Figure 3. Stimulated emission traces of HBDI at 525 nm. The data have been normalized at the minimum. Solid lines show the fit curves obtained using the model depicted in Figure 8 and the parameters given in Table 1.

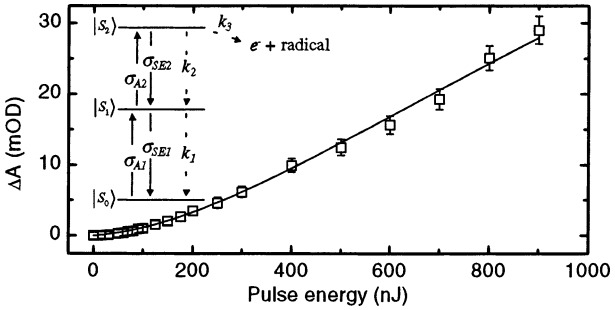

Figure 4. Excitation pulse energy dependence (squares) of the difference absorption signal in HBDI at pH = 10. Detection wavelength, 620 nm; delay time, 20 ps. The solid line shows modeled power dependence using the model depicted in the inset. The solid arrows indicate absorption and stimulated emission with corresponding cross-sections σ, and dashed arrows stand for spontaneous processes occurring with rates k. For more details on the modeling see ref 33.

HBDI at pH = 10. At low excitation densities, the power dependence exhibits a quadratic trend; however, as the excitation power increases, it straightens out and becomes linear. This pseudolinear trend is discussed and analyzed below.

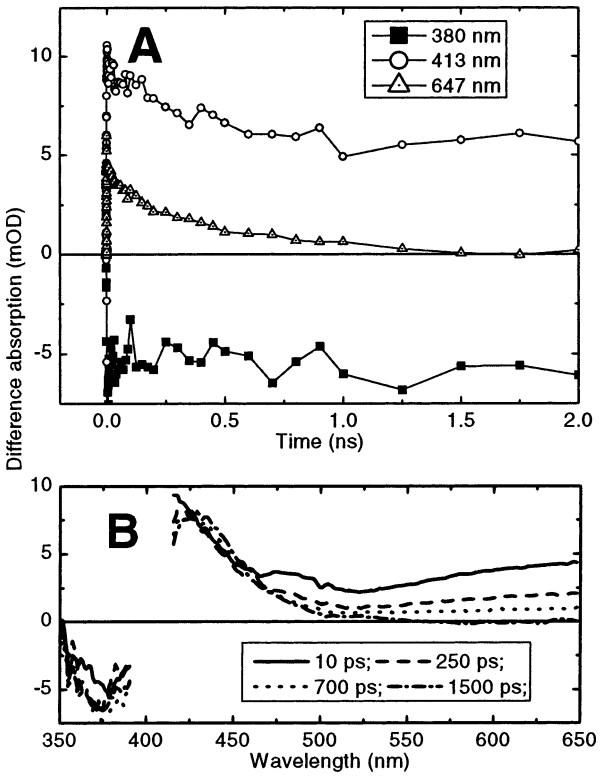

Figure 5. Slow dynamics of the difference absorption of HBDI at pH 1. A: Pump−probe traces at the maximum of GSB (solid squares), radical band (open circles), and solvated electron band (open triangles). B: time gated spectra at different delay times. Solvated electron signal (broad band in the red) disappears while the GSB and the induced absorption due to the radical remain.

3.2. Pump-Dump-Probe Data. Since the PP data are qualitatively similar for all studied solutions (at least spectrally), we describe the PDP experimental results for the pH 10.5 aqueous sample only. A multiwavelength comparison of the studied samples will be further explored in the Discussion. In Figure 6, representative PP (unfilled squares) and PDP (unfilled circles) traces measured in the anionic HBDI sample at the different wavelengths are contrasted. The 530-nm dump pulse is applied at 250 fs following the 400-nm pump pulse and affects the transient absorption signals at all probed wavelengths. Upon dumping, a ∼40% loss of the SE is instantly observed (550 nm) due to the reduction of the excited-state population.

A similar dump effect is observed in the induced absorption observed in the UV (362 nm); at this probe wavelength, a smaller (20%) loss is observed immediately after the dump pulse. This is in agreement with ascribing this positive band to an ESA band that overlays and dominates the GSB in this spectral region. Since at this wavelength the PP signal is a combination of several overlapping bands with differing signs (e.g., ESA, GSB, and terminal spectrum), ascertaining the dumping efficiency is difficult without the global analysis of the complete wavelength-resolved data set. The PDP signals of the GSB (420 nm) exhibit similar behavior, the difference signal instantaneously becomes negative, increases until reaching a positive maximum at ∼800 fs, and then decays with a ∼2 ps lifetime. The initially negative ΔΔOD signal results from a loss of overlapping ESA (positive PP signal), whereas the positive ΔΔOD is a delayed refill of the GSB (negative PP signal).

In contrast to the decrease of the UV ESA band (362 nm), the induced absorption band observed at 470 nm exhibits an instantaneous *increase* of the signal. The ΔΔOD signal in Figure 6 shows an instrument limited rise followed by a 600 fs decay.

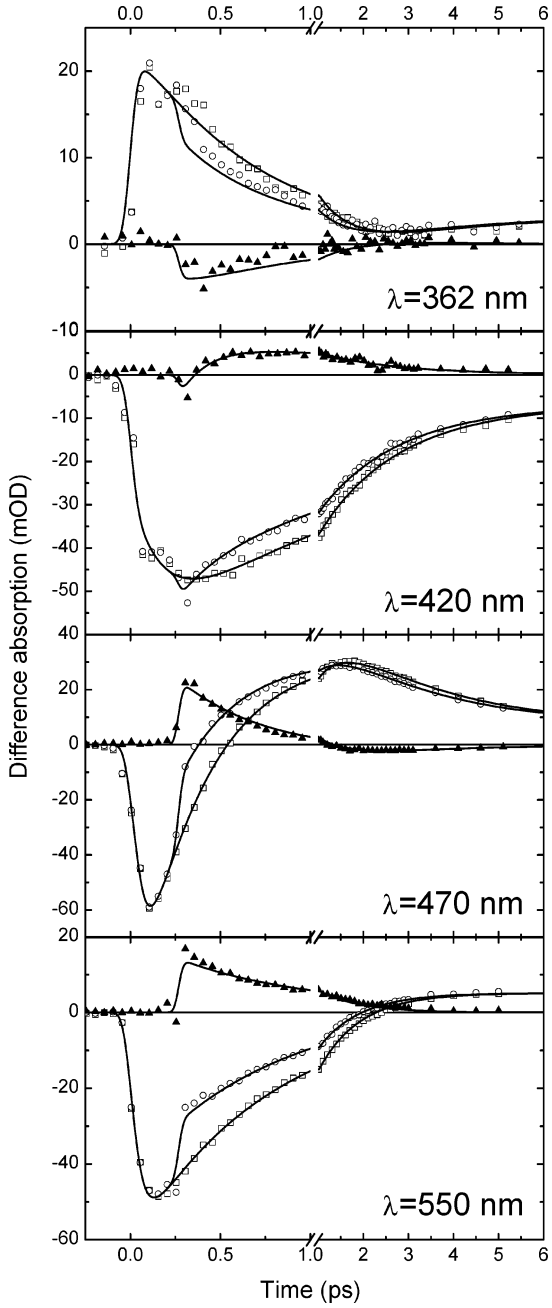

Figure 6. Pump−probe (squares), pump−dump−probe (circles), and the difference between the two (triangles) traces of HBDI (pH 10.5) at 362, 420, 470, and 550 nm. Solid lines represent the global fit of the data using the model described in the discussion section. Dumping time was ca. 270 fs.

This is not the signature of an ESA, but of a transient species that is further generated by the dump pulse: a ground-state intermediate (GSI). This assertion is further reinforced by the observation of a negative ΔΔOD signal at longer times (∼2ps), which results from a "loss" of induced absorption that would be there in the absence of the dump pulse. Though the observed increase in this probe wavelength can be partially explained by the dump effects from the overlapping SE band (550 nm), the global analysis results show a clear separation (and clear spectral differences) between the increase due to the depletion of the SE and the increase of the GSI.

Although a clear dump-induced change in the PP signals is observed at all probe wavelengths immediately after the dump pulse, no resolvable dump effect is observed at later probe

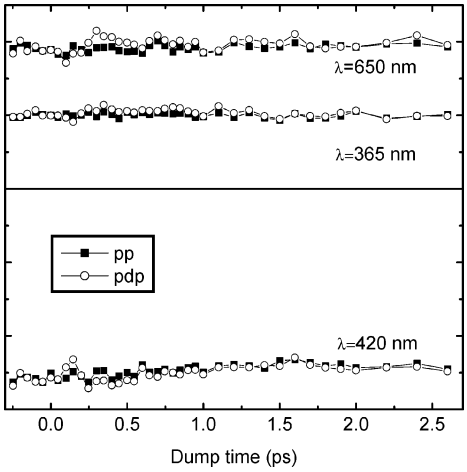

Figure 7. Pump−dump−probe action traces at different wavelengths of HBDI in water at pH 10.5. The probe time was 50 ps.

delays, when only the terminal spectrum is observed; the ΔΔOD signals decays to zero with no persistent depletion. This can be partially observed in the ΔΔOD signals of Figure 6; however, this effect is better observed in data collected differently.

The PDP data discussed above are in the form of "kinetic traces," where the dump pulse was fixed at a specific time (270 fs) and the delay of the probe pulse was varied generating the observed data. However, "action trace" data are collected with an alternative timing scheme, where the probe pulse is fixed at a specific time and the delay of the dump pulse is varied.[33,41] While the kinetic trace data measure the dynamics of the transient states directly as they evolve (with or without the dump pulse), the action trace data measures the asymptotic effects, if any, of the dumping process of a specific probe time and spectrum. Action traces are particularly useful for determining the connectivity scheme underlying the PP signals.[28,33]

The action trace data measured for the high pH HBDI sample, probed at 50 ps, are compared in Figure 7. As the long time ΔΔOD signals suggest in Figure 6, no appreciable effect is observed on the terminal 50 ps spectrum, regardless of the delay of the dump pulse. This lack of a dump effect demonstrates clearly that the species responsible for the terminal spectrum observed at 50 ps do not evolve via the excited state that is depleted by the dump pulse. Hence, the connectivity scheme describing the observed PP signals is not exclusively sequential but must include a branching.

4. Discussion

4.1. Photoproducts. The "terminal" spectra observed in the PP signals show that long-living photoproducts are generated upon excitation of HBDI in solution at all three pHs (Figure 2B,D,F,H dot−dashed curves) that persist for the duration of the experiment (>4 ns). These spectra exhibit similar features: (1) a broad positive band peaking to the far red of the probe windows, (2) a negative band attributed to the GSB, and (3) a narrow band peaking just to the red of the GSB (i.e. 470, 425, and 400 nm for the pH 10.5, 5, and 1 solutions, respectively). By comparing the GSB at early (200 fs) and late (10 ps) probe times, we estimate that the yield of this photoproduct under our experimental conditions ranges from 10% to 25% depending on pH.

Since the ultrafast excited state quenching presumably originates from ultrafast internal conversion due to torsion around the double bond backbone of the free chromophore in solution (Figure 1), it is tempting to ascribe these terminal spectra to photoisomerized HBDI molecules.[42] However, the absorption spectra measured for the cis and trans isomers of the HBDI chromophores share similar spectral properties, although with slightly different extinction coefficients.[31] Moreover, this assignment does not explain the origin of the broad band in the red, nor why the spectra are not affected by the presence (and timing) of the dump pulses (Figure 7), a property expected for a product resulting from excited-state isomerization.[43] It also does not explain the observed pseudolinear excitation intensity dependence of the spectrum of the terminal photoproducts in Figure 4. A more plausible explanation for this persistent spectrum is that the pump laser pulse ionizes some of the HBDI chromophores, which eject electrons into the surrounding solvent where they are subsequently solvated;[44,45] this process also results in HBDI radicals. The broad induced absorption band in the red part of the terminal spectrum is similar to the previously observed hydrated electron spectrum,[46] suggesting that the narrow band overlaying the red part of the GSB is associated with the concomitantly generated radical species.

Similar nonevolving terminal spectra have been observed in other molecules containing the phenolic moiety, including model PYP chromophores,[33,47,48] another GFP chromophore analogue,[22] and other small aromatic chromophores.[49] Since the excitation energy at 400 nm (25 000 cm^{-1}) corresponds to the manifold of the bound electronic states of HBDI, which presumably is lower than the expected ionization threshold for organic molecules, the photoionization consequently results from a multiphoton process. The observed dependence of radical yield on the excitation intensity further confirms that this process results from the absorption of multiple photons (Figure 4). This power dependence is quadratic only at very low excitation pulse energies; later it straightens out, indicating that the ionization proceeds via a sequential two-step absorption process (where the second photon is absorbed by the excited state created by the absorption of the first photon).[28] The solid line in Figure 4 depicts a modeled power dependence using the three-state model shown in the inset. A near identical power dependence with the same spectral features of hydrated electrons has also been observed before in the PYP model chromophore[33,50] and other ionizing chromophores.[51]

The extended persistence of the terminal spectra is partially dictated by the electron-radical recombination kinetics,[52,53] which is a diffusion-limited reaction occurring on time scales longer than our experimental window. However, the solvated electron band in the pH 1 sample exhibits a pronounced decay on a ~400 ps time scale (Figure 5), whereas the coexisting radical and GSB bands do not. Since free protons are known scavengers of hydrated electrons,[54,55] we ascribe this decay of the hydrated electron band to the scavenging dynamics of free protons and electrons, which is most noticeable in the elevated proton concentration found in the pH 1 sample. Since this reaction does not involve the radical species, neither the GSB nor the radical band are affected. No appreciable degradation of the HBDI absorption spectrum is observed in all solutions following the measurements, indicating that the generated radical species eventually recombine with the ejected electrons. A persistent GSB has been observed in other single-wavelength PP experiments on the HBDI chromophore, which may be ascribed to the ionization pahway.[13]

A similar ionization process may potentially take place in ultrafast experiments with the GFP chromophore bound within the protein environment. As with HBDI in solution, ionized radicals and "solvated" electrons would be generated. Several dispersed PP experiments on GFP do show signs of this

interfering ionization pathway. Induced absorption to the red edge of the GSB (~430 nm) has been observed;[26,56] though ascribed to an ESA, this may be partially explained by the presence of a radical absorption band. Also, a persistent induced absorption was observed to the red of the SE band of GFP, which is similar to the solvated electron bands in Figure 2.[56] In PYP, the fast quenching of the excited state allows for the observation of this pathway; in contrast, the long-lived excited state of GFP masks this potential contribution to the signals. A PDP study exploring this ionization possibility in the GFP protein is currently in progress.

4.2. Phenomenological Model. The PP dynamics observed in HBDI is typical of solvated chromophores that twist upon excitation.[18,33,57,58] After excitation of the HBDI chromophore, the conjugation of the π-electron system is modified, resulting in greater rotational freedom around one or more double bonds.[20,25] As the chromophore evolves on the excited-state potential energy surface (via the twisting coordinate), the energy difference between the ground and excited state decreases, resulting in enhanced internal conversion.[59] Moreover, ab initio studies of similar twisting molecules have shown that conical intersections play a significant role in further enhancing the internal conversion rate.[18,60,61]

Ideally, the twisting of the chromophore results in a time-dependent energy difference between the ground and excited electronic states that would be manifested as a red-shifting of the observed fluorescence and SE (assuming a barrier-less potential energy surface).[62−68] However, since time-resolved studies of such chromophores are generally performed in solution, potential solvent effects may obscure this observation. Upon excitation of the chromophore in solution, the surrounding solvent molecules, which were initially equilibrated with the ground electronic state of the solute, are in a nonequilibrium state and will adjust their positions and dipole moments in order to accommodate the changed properties (e.g., dipole moment or polarizability) of the new electronic state.[69,70] The solvation dynamics is driven by a decrease of the total energy of the solvent−solute system and as a result, any measurement that probes the transition energy will mirror the underlying solvation dynamics of the system.[70] Hence, both solvation dynamics and molecular twisting would contribute to any observed red-shifting of the SE band.[64,65] Consequently, ascribing the red-shifting dynamics into either isomerization or solvation categories requires care.

These contributions are not limited to excited-state dynamics but are also applicable to the ground-state dynamics observed in the PDP data here. When the twisting excited-state chromophores are dumped to their ground state, their nuclear configurations (and those of the surrounding solvent molecules) are no longer energetically optimal. Hence, evolution on the ground-state potential energy surface is the reverse of the excited state evolution; the molecule rearranges its nuclei back to the original ground state configuration and the solvent molecules also rearrange accordingly (ground-state solvation).[67] Although usually excited-state isomerization dynamics is rationalized with a one-dimensional reaction coordinate, in reality it can be multidimensional and include the twisting of several bonds[18,71] along with the rearrangement of solvent molecules. The effects of such multidimensionality will be discussed below.

The modeling of the PP signals alone does not provide a clear separation of decay time scales and spectral signatures of the ground transient states; to accomplish this, the simultaneous fitting of both PP and PDP data is required. The information yielded by PDP experiment provides valuable insight in the ground-state dynamics and reveals the origin of different overlapping bands. When the dump pulse de-excites the excited HBDI molecules in the "semi-twisted" (or "semi-solvated") state, the SE is depleted, and concomitantly, the nonequilibrium ground-state absorption at 470 nm increases (Figure 6). This provides a qualitative explanation for the differences in the PDP kinetics between the two induced absorption bands peaking at 362 and 470 nm (Figure 6). Although the UV band is a true ESA (along with the radical band underneath it) and *disappears* upon dumping, the 470 nm band is due to the absorption of unrelaxed ground-state species, which *increases* upon dumping. Immediately following the excitation, the PP signal at 470 nm is dominated by the SE, but as the excited state is quenched by twisting (and shifts to the red), the absorption from the unrelaxed ground state at 470 nm increases.

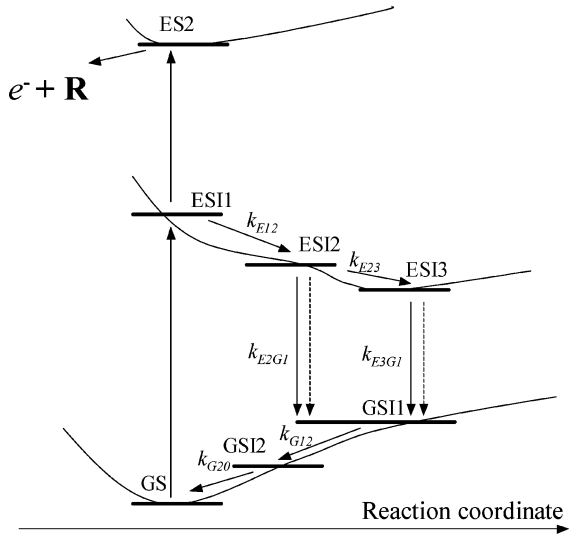

Figure 8. Connectivity scheme used for the analysis of the photodynamics of HBDI. ESI1, ESI2, and ESI3 denote discrete excited-state intermediates. GSI1 and GSI2 are the ground-state intermediates, representing the unrelaxed ground state. The rate constants used for the modeling are indicated beside the corresponding arrows. Dashed arrows indicate the action of the dump pulse.

In the applied model, we need to account for both one-photon dynamics with evolution along the excited and ground electronic states and the competing two-photon ionization. The ionization process is introduced as an additional pathway that is initiated within the excitation pulse and evolves in parallel with the single-photon dynamics. Even though electron relaxation dynamics (<1 ps), as the water molecules solvate the ejected electrons has been previously observed,[44,72] such spectral evolution was not discernible in our data (apart from electron scavenging and recombination occurring on considerably slower time scales in the pH 1 sample) and was not included in the modeling. This simplification captures the essence of the ionization process and its interfering contributions to the single-photon dynamics.

On the basis of the above considerations, we use the connectivity scheme shown in Figure 8 to analyze the measured PP and PDP data. From Figures 2 and 6, it is evident that, to explain the main features of the data, the model has to include at least three components: (1) solvated electron and radical that results in the terminal PP spectrum, (2) emissive state that is responsible for the stimulated emission and induced absorption bands, and (3) unrelaxed ground state that is created either by the dump pulse or by natural decay from the emissive state (470 nm trace in Figure 6). The kinetics of the SE band (Figures 2 and 6) is slightly different from that of the ESA band and

nonuniform across the SE spectral region from 550 to 650 nm, which indicates that the excited-state evolution should involve more than one compartment with different ESA and SE properties. In fact, due to solvation effects, vibrational relaxation, etc. (see above), excited-state dynamics on a ps time domain almost *always* involves more than one exponential component.[63,64,73] Moreover, quantum calculations on the GFP chromophore in solution suggest that a nonexponential quenching behavior is inherent to the HBDI chromophore.[74] Multiple exponential excited-state quenching has earlier been observed in time-resolved fluorescence signals of HBDI or other GFP model chromophores.[17,21] Also, at wavelengths between 500 and 550 nm, the dump-induced effect immediately after the application of dump pulse is not only a loss of SE (normalized traces not shown) but involves the formation of a nonequilibrated ground-state species. Thus, introducing a ground-state intermediate, absorbing to the red of the GSB, is required to describe the PDP data. Considering these features of the data, we arrive at the model shown in Figure 8. The evolution on excited-state potential energy surface is represented by three discrete compartments, the ground-state evolution involves two discreet intermediates.

Alternative models can be postulated to interpret the observed PDP data; however, the model presented here has resulted from a careful search among many possible models, based on three criteria: 1) adequate description to the data, (2) minimum possible number of compartments, and (3) plausible resulting SADS corresponding to our intuition as to the excite-state dynamics of the molecule. Other, more complex, models can be constructed to fit the data, but the one shown in Figure 8 has a minimum number of compartments. If one or more of the compartments are left out, the residuals of the fit show considerable structure and the fit becomes unsatisfactory.

4.3. Excited and Ground-State Evolution. This model fits both the PP and PDP data well (Figures 3 and 6) and provides a basis for understanding the complex photoinduced dynamics in HBDI. The corresponding SADS and decay time scales estimated from the global analysis of each sample are shown in Figure 9 and Table 1, respectively. The first excited-state intermediate, ESI1, represents evolution from the Franck−Condon region with an instrument limited decay (∼50 fs) for all samples except the high viscosity glycerol mixture; the two remaining excited-state intermediates, ESI2 and ESI3, evolve on slower time scales. The SADS of the ESI1 has been strongly contaminated by the coherent artifacts (e.g., cross-phase modulation and stimulated Raman scattering) and is omitted in Figure 9. Both ESI2 and ESI3 relax to the first ground-state intermediate, GSI1, either via internal conversion or by the applied dump pulse (in the PDP data). Subsequently, GSI1 relaxes into GSI2 and then GSI2 decays into the original ground state to fill the GSB.

Only in the pH 10 data can the spectral differences be distinguished between ESI2 and ESI3. At pH 5 and pH 1, the spectra of these intermediates are near identical and are set to be the same in the global analysis routine to improve the robustness of the analysis. Hence, little spectral evolution is observed in the excited state, and the SE decays in a biexponential fashion in agreement with previous measurements.[75] In the pH 10 sample, a weak red shift and narrowing of SE is observed in the transition from ESI2 → ESI3 (Figure 9, black and red curves). The ESI2 evolves to ESI3 in 520, 210, and 660 fs for pH 1, 5, and 10.5, respectively. The ESI3 decays in 750, 420, and 940 fs, respectively. The presence of the 80 fs component (ESI2 to GSI1) at pH 5 reflects the fact that as soon as the coherent artifact is over, the GSI1 is already observed (Figure 2B). The rate of the GSI2 decay follows the same order for all three pH values as the excited-state decay: 1.4, 1.3, and 2 ps. Both the GSI1 and GSI2 exhibit absorption bands to the red of the GSB (Figure 9, blue and green curves) with the short-lived GSI1 absorbing further to the red than GSI2. The magnitude of the GSB band in the GSI1 SADS is larger than

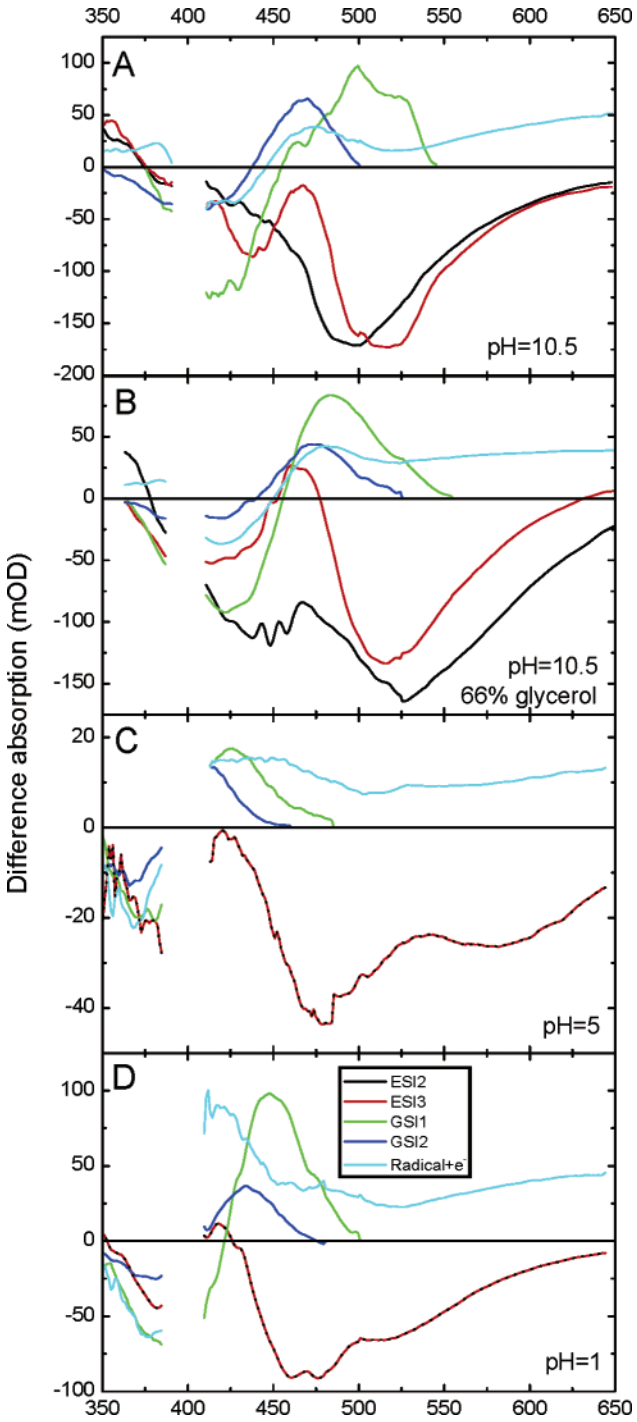

Figure 9. SADS resulting from the global fit of pump−dump−probe data on HBDI at, pH 10.5 water buffer (A), pH 10.5 water/glycerol mixture (B), pH 5 (C), and pH 1 (D). The associated rate constants are given in Table 1. The SADS of the ESI1 have been strongly affected by the cross phase modulation between the pump and probe pulses, hence they have been omitted from the plots. The spectra of ESI2 and ESI3 have been set to be equal at pH 5 and pH 1 (they are represented by black-red lines). The legend in panel D applies to all figures.

TABLE 1: Rates of Different Reactions Represented by Arrows in Figure 8[a]

global fits	inverse rate	pH 1	pH 5	pH 10.5	pH 10.5, 66% glycerol
excited-state evolution	$1/k_{E12}$	50 fs	50 fs	50 fs	140 fs
	$1/k_{E23}$	520 fs	210 fs	660 fs	1.2 ps
excited-state decay	$1/k_{E2G1}$	390 fs	80 fs	620 fs	1.2 ps
	$1/k_{E3G1}$	750 fs	420 fs	940 fs	4.7 ps
ground-state evolution	$1/k_{G12}$	380 fs	470 fs	170 fs	1.4 ps
	$1/k_{G20}$	1.4 ps	1.3 ps	2 ps	3.7 ps

[a] Only in the glycerol-containing solvent, the time resolution of our instrument (120 fs) was enough to resolve the lifetime of ESI1. In all of the other cases, it was fixed to 50 fs. The uncertainties of the parameters were below 20% (typically around 10%) for the other time constants.

that of GSI2 (Figure 9) which is a consequence of the greater overlap of GSI2 with the GSB than GSI1.

The spectral region just to the longer wavelength of the GSB is a particularly difficult region to model properly. In this spectral window, there are at least three different bands contributing: absorption from the radical and solvated electrons, GSIs, and possibly an ESA band from both ESI2 and ESI3. In the same region, at least at the early probe times, there is also some overlap with the negative SE band. Several of the time constants extracted are comparable with the time-resolution (125 fs). Hence, even though the model describes the data well in this region, it is hard to exclude the possibility that the induced absorption here is entirely due to the absorption of the GSIs formed already at the times immediately after the excitation.

To identify the nature of the observed GSIs, we compare the dynamics of HBDI in a 66% mixture of glycerol in water to the observed dynamics in pure water (both at pH 10.5). In the glycerol/water mixture, the evolution is slowed considerably (Table 1). The ESI2 evolves to ESI3 in 1.2 ps, the slowest step in the excited-state decay is 4.7 ps, and the "fast" and "slow" GSIs decay in 1.4 and 3.5 ps, respectively. The rates are slowed 2−5 times. From a mechanistic perspective, the expected rate would be proportional to the viscosity.[13,21] Since the viscosity of the glycerol-containing solvent is ∼26-fold greater than the pure water samples, the bulk viscosity is not a useful parameter to model the quenching time of HBDI.[71] A similar weak viscosity dependence for HBDI was observed in ultrafast fluorescence upconversion measurements and was ascribed to the volume-conserving hula-twist mechanism.[13]

4.4. Reaction Coordinate. The model used in the global analysis in Figure 8 describes well the excited state and ground state evolution in the measured PP and PDP data (Figures 3 and 6). However, the nature of the reaction coordinate is not explicitly assumed. Different dynamical effects contribute to the observed dynamics including multidimensional twisting motions (i.e., hula-twist[23,24] or two-bond flip), excited and ground-state solvation dynamics and vibrational cooling.

Solvation dynamics is manifested in the PP (and time-resolved fluorescence) experiments as a dynamic red shifting of the emission[62−67] and often occurs in a multiphase manner, including a sub-200 fs response accompanied with slower ps phase.[62,76,77] Previously measured solvation time scales in aqueous solutions are approximately 55 fs with 128 and 880 fs relaxations.[63,78] Similar signatures of solvation dynamics have been observed in other isomerising chromophores of biological proteins: the pigment of PYP[33] and the protonated Schiff base from bacteriorhodopsin.[58] The observed excited state lifetimes in these chromophores were significantly longer than that of HBDI. In the anionic HBDI chromophore, only a slight red-shifting is observed during the ESI2 to ESI3 evolution and the blue-shift during GSI1 to GSI2 evolution. This may be (partly) due to solvation dynamics. Furthermore, no significant shifting of time-resolved fluorescence has been observed for HBDI in both alcohol[17] and aqueous solutions.[79] In fact, the ESI1 to ESI3 dynamics is better described as narrowing, not shifting, of the SE band (especially at pH 10.5). Ultrafast upconversion measurements performed on PYP protein samples[80] also show a similar narrowing, with little or no shifting.

Electrooptic Stark experiments estimate the change in the dipole moment of the chromophore in the GFP protein following excitation to be ∼6.8 D for the protonated form and less than 20 D for the deprotonated form.[8] Ab initio calculations of the ground and excited-state dipole moments suggest a small (∼2 D) change in dipole moment of both the neutral and anionic HBDI chromophore.[81] These are corroborated by Stark experiments on the neutral chromophore in a GFP mutant.[82] Consequently, no significant spectral shifting (i.e., solvation dynamics) is observed in either ultrafast PP or fluorescence upconversion experiments[17] that monitor excited-state dynamics in HBDI. Within the linear response approximation,[67,83] the ground-state solvation would also exhibit similar dynamical behavior as the excited-state dynamics. Small differences between excited- and ground-state solvation have been observed, suggesting that the ground-state solvation time scales may be faster than those of the excited-state solvation.[67] In contrast, for HBDI, the ground-state time scales are distinctly slower for HBDI than the excited-state dynamics (Table 1). Thus, we exclude ground-state solvation dynamics as a major contributor to the observed dynamical shifting between GSI1 and GSI2 (Figure 9) in HBDI.

Vibrational cooling and intramolecular vibrational relaxation (IVR) are alternative mechanisms that could potentially contribute to the observed ground-state dynamics. In these ultrafast experiments, the HBDI molecules are excited with a 400-nm photon, imparting 25 000 cm^{-1} of excitation energy into the chromophore. After internal conversion, this excitation energy must be dissipated in the form of vibrational cooling from the "hot" ground-state chromophore to the solvent molecules. The signature of a hot chromophore is an absorption band that is red-shifted from the ground-state absorption spectrum,[84] which relaxes to fill the GSB. This is similar to the observed ground-state dynamics observed for HBDI in Figure 9.

Previously observed time scales for vibrational cooling of similar sized molecules are of the order of 10 ps,[84,85] which are considerably slower than the observed ground-state evolution of HDBI (Table 1). These vibrational cooling time scales are also not significantly affected by varying the solvent properties;[85] the ground-state evolution for HBDI dissolved in the 66% glycerol solution, with a 26 times higher viscosity, exhibits appreciably slower dynamics than the aqueous solution. In the PDP experiments, the dumping of the excited state increases the population of the GSI bands (Figure 6), even though approximately 75% of the initial excitation energy is removed by the stimulated emission photons. This would result in less vibrational energy introduced into the nascent ground state species and hence reduced GSI amplitudes. However, the PDP and PP data could be simultaneously fit with the model using the same spectra for the GSIs, irrespective of the mechanism of generation (i.e., natural quenching or dumping with a laser pulse).

IVR generally occurs on a faster time scale than vibrational cooling and may also result in spectral evolution similar to the one observed here; it provides no explanation for the rapid excited-state quenching nor the previously observed temperature

dependence[14] of fluorescence, nor viscosity dependence of pump−probe. Although we cannot exclude the possibility that vibrational cooling or IVR contributes to the ground-state dynamics of HBDI, these observations suggest that it is not a significant factor. This leaves the structural rearrangement of the molecule as the main mechanism responsible for the observed ground and excited-state dynamics. Although structural rearrangement can also be viewed as the vibrational (or IVR) relaxation along the reaction twisting coordinate, especially during ultrafast time scales such as those observed here, for the sake of discussion, we separate the two as distinct processes. Excitation-wavelength-dependent PP and PDP measurements are in progress to further explore this aspect.

Upon excitation, the HBDI molecules evolve on the excited state potential surface, resulting in a twisting around one or more bonds, which enhances the internal conversion. Once these twisted molecules are in the ground-state, they subsequently evolve back into the original nontwisted equilibrium geometry. In a simple one-dimensional model used to interpret this twisting, rotation occurs as a consequence of weakening of the double bond after an electronic transition (e.g., via a $\pi \rightarrow \pi^*$ transition).[18,71,86,87] If the downward slope of the excited-state potential along the rotation coordinate is flatter than the ground-state potential, then the observed excited-state dynamics would be slower than the corresponding ground-state dynamics. For the GFP chromophore, such potential energy surfaces have been predicted.[25,88] This reaction rate difference would be even larger if a barrier were to hinder the twisting dynamics in the excited state. Excited-state barriers have been proposed for other isomerising systems including *trans*-stilbene,[89] a model PYP chromophore analogue,[90] and the isomerization of the Schiff base in the bacteriorhodopsin protein.[91−93] In a similar dispersed PDP experiment on the PYP chromophore in solution, the ground-state lifetimes were shorter than those for the excited-state quenching;[33] comparable differences have been observed in molecules exhibiting twisting-induced charge-transfer reactions.[57]

In contrast to these studies, the ground-state dynamics in HBDI is slower than that of the excited state and this merits some explanation. Two explanations are postulated: (1) the ground-state potential may have an appreciable energy barrier (or more complex dynamical evolution) that must be overcome as the system relaxes or (2) the same reaction coordinate is not shared for evolution on both electronic states. The PDP data and kinetic model presented here do not distinguish between these two potential explanations. The first explanation is the simplest, where the ground-state potential exhibits an energy barrier that the nascent ground-state HBDI molecules must surpass.[88,94] In this scenario, multiexponential dynamics would be expected.

The other explanation requires multiple structural evolution along more than one rotational degree of freedom (e.g., a hula-twist mechanism[23]), which was earlier proposed for explaining the ultrafast polarization measurements of HBDI.[14] When multiple dimensions are considered, the structural evolution along the excited-state pathway needs not coincide with the return evolution along the ground state potential and may result in different dynamics. Because different trajectories in the ground and excited states may exist, it would be impossible to properly define a one-dimensional reaction coordinate as illustrated in Figure 8. The fact that the dynamics are so different between the excited state and the ground-state highlights the complexity of the HBDI photoinduced dynamics. Previously, a three state model was proposed to explain the lack of spectral evolution in the excited-state signals for the bacteriorhodopsin protein,[91] involving the interplay of three different electronic states, though the applicability of this model to the HBDI is suspect since ab initio calculations do not show multiple excited electronic state that intersect.[20,25] Meech and co-workers recently employed a two-coordinate model that includes both a vibrational and a twisting coordinate to explain the ultrafast time-resolved fluorescence measurements on HBDI in different solvents.[75] Since no ground-state energy barrier has been predicted for HBDI and similar chromophores, the complex multidimensionality of the reaction pathway is more likely the underlying reason for the different dynamics between the ground and excited-state evolution.

It has been postulated that in some excited-state isomerization reactions, the observed quenching time scales in the ultrafast experiments may be ascribed not only to a loss of excited state population, but also to a decreasing emission transition dipole moment as the excited-state population evolves along the potential energy surface until the excited state becomes effectively a "dark" state.[43,57] If this is also applicable for the GFP chromophore, as the molecule twists, the excited state population would evolve into a lower-energy dark state before internally converting to the ground state, and consequently, the ESII would have a higher emission dipole than ESI2, which would be correspondingly higher than ESI3. However, the results from the global analysis using the applied model do not strongly support this hypothesis, since the observed ESI3 state has a strong transition moment. Moreover, it seems that the GSI1 is created without any delay from ESIs. Hence, the introduction of an unseen hidden state is not required to describe the population flow across the excited- and ground-state surfaces. However, it may be possible that a dark state exists but is very short-lived and does not accumulate appreciable population and thus the PP and PDP data (and modeling) are simply not sensitive to it. Ruhman and co-workers applied the PDP technique to identify that the transition dipole moment for emission does not vary in time for the isomerization of the retinal chromophore in bacteriorhodopsin.[43]

4.5. pH Dependence. The HBDI chromophore closely resembles model PYP chromophores; both have a phenolic moiety and share similar conjugated π electron systems.[33,47] Levy and co-workers have performed excitation wavelength-dependent fluorescence measurements on a PYP chromophore analogue in the gas phase[95] and found signs of an excited-state energy barrier. This was reaffirmed by recent ab initio calculations of Martínez and co-workers.[90] A similar barrier has been suggested to exist for the GFP chromophore from experimental studies[14,15] and theoretical computations.[20,25]

The behavior of HBDI at different protonation states are qualitatively similar (Figure 8), with the same sequence of ground and excited state intermediates but with differing time scales. The excited state and ground-state lifetimes (Table 1) are strongly correlated with the position of the absorption maximum (Figure 1); the excited-state quenching is fastest in the neutral form of HBDI (with the blue-most absorption maximum), followed by the cationic form (pH 1), and then the anionic form (pH 10.5) is the slowest. This trend is the opposite of what one would expect if a large energy barrier was present for excited-state twisting (and hence quenching): the neutral HBDI chromophore exhibits the fastest quenching, but also has the least excess energy imparted by excitation. Analogously, the HBDI anion is the slowest but has the most excess energy. Presumably, the excess energy would contribute to overcoming excited-state barriers,[18] and the protonation state with the most

excess energy would exhibit the fastest excited state quenching. Thus, we suggest that the observed dependence of rates on pH results from the specific changes to the potential energy surfaces from the protonation and not necessarily from the amount of excess energy introduced to the chromophore.

Several quantum calculations have explored the effect of protonation on the resulting potential energy surfaces. Weber et al.[25] and Voityuk et al.[96] simulated the ground and excited electronic potential energy surfaces for the GFP chromophore analogue in a vacuum and showed that the reaction mechanism for twisting depends strongly on the protonation state. Although both studies show clear protonation dependences, they disagree in identifying about which bond(s) the twisting occurs for the same protonation state. The Weber et al. study suggests that, for the anionic form, the excited state potential energy surface is nearly flat for the separate bond flips (for either the single bond next to the phenolic ring or the double bond next to the imidazolinone ring), whereas the double-bond hula-twist flip mechanism shows an excited state barrier. In sharp contrast, the excited state surface for the neutral chromophore is barrierless for both the single bond flip and the hula-twist. This is in agreement with the results presented here, where the neutral form is quenched considerably faster than the anionic form. Unfortunately, these authors did not consider the cationic chromophore in their study. In contrast, the excited-state potentials calculated in the Voityuk et al. study, which considered only single bond flips, exhibit properties that are different than the Weber et al. surfaces. In their study, the authors observed a clear energy minimum in the excited-state surface for the anionic form, whereas the surface calculated for the neutral species appears flatter. This conflict in quantum mechanical calculations highlights the complexity of the quenching dynamics of the GFP chromophore and the need for more elaborate theoretical studies.

The correlation between the absorption maxima and the observed rates of excited and ground-state evolution suggests that perhaps it is the coupling of the chromophore to the solvent that determines the excited and ground-state reaction rates. This coupling might be sensitive to the charge distribution in the molecule, which would explain why anionic and cationic forms of the pigment are more similar to each other than to the neutral form. Recently, Martínez and co-workers extended the quantum mechanical/molecular mechanical (QMMM) technique to study the quenching and isomerization dynamics of HBDI in a vacuum and water[97] and observed that the polar solvent environment shifts the conical intersection into the pathway of the twisting coordinate which leads to enhanced internal conversion. It may be hypothesized that the coupling to the environment (caused by the chromophore charge distribution) modulates the position of the conical intersection with respect to the twisting coordinate and hence affects the quenching time scales. An analogous conclusion was drawn from similar ab initio calculations on the photoactive yellow chromophore in vacuum and in the protein.[98]

A clear understanding of why the protonation state modulates the quenching time scales of HBDI is lacking. Additional PDP experiments, performed in different solvents and with variable substitutions on the HBDI chromophore, coupled with detailed computational efforts would hopefully shed light on this issue.

5. Summary

Using wavelength and time-resolved pump−probe and pump−dump−probe spectroscopy, the excited and ground-state photoinduced dynamics of the GFP chromophore, HBDI, was investigated. Additionally, the influence of the protonation state and the solvent viscosity on these dynamics was studied. Upon ultrafast excitation of HBDI, two pathways of evolution are observed: a one-photon twisting pathway and a two-photon ionization pathway. The two-photon photoionization process results in the generation of two species that interfere with the one-photon transient states: a hydrated electron and a corresponding radical, both featuring the corresponding induced absorption bands and the concomitant ground-state bleach. The one-photon pathway includes a cyclic photoreaction that involves several excited and ground-state intermediates. The proposed reaction scheme (Figure 8) quantitatively describes the measured signals for all protonation states, though with pH dependent time constants (Table 1). No clearly resolved solvation dynamics are observed as a shifting of the stimulated emission, in contrast to similar PYP chromophores. The neutral HBDI form exhibits the fastest dynamics, followed by the cationic and then anionic forms. The observed kinetics are further slowed dissolving HBDI in the more viscous 66% glycerol/water solvent, though not to the magnitude expected from the 26-fold increase in viscosity of the solution. The slower dynamics seen for the ground-state evolution vs the excited state is perhaps the consequence of the two-bond flip (i.e., hula-twist) nature of the twisting reaction. Despite this, no clear fully isomerized HBDI photoproducts are observed, suggesting the yield for isomerization is lower than the experimental sensitivity (∼5%).

Acknowledgment. Sincere thanks to Prof. Todd Martínez (U. Illinois at Urbana-Champaign), Prof. Stephen Bradforth (U. Southern California), and Prof. Stephen Meech (U. East Anglia, UK) for constructive discussions and for the sharing of recently published results. This research was supported by The Netherlands Organization for Scientific Research (NWO), Netherlands via the Dutch Foundation for Earth and Life Sciences (ALW). M.V. was supported by The Netherlands Organization of Fundamental Research of Matter (FOM). D.S.L. is grateful to the Human Frontier Science Program Organization for providing financial support with a long-term fellowship.

References and Notes

(1) Prendergast, F. G. Biophysics of the green fluorescent protein. In *Methods in Cell Biology*; Academic Press: San Diego, CA, 1999; Vol. 58; p 1.
(2) Tsien, R. Y. *Ann. Rev. Biochem.* **1998**, *67*, 509.
(3) Zimmer, M. *Chem. Rev.* **2002**, *102*, 759.
(4) Prasher, D. C. *Trends Genet.* **1995**, *11*, 320.
(5) Haseloff, J.; Siemering, K. R.; Prasher, D. C.; Hodge, S. *Proc. Natl. Acad. Sci. U.S.A.* **1997**, *94*, 2122.
(6) Cody, C. W.; Prasher, D. C.; Westler, W. M.; Prendergast, F. G.; Ward, W. W. *Biochemistry* **1993**, *32*, 1212.
(7) Warren, A.; Zimmer, M. *J. Mol. Graph. Model.* **2001**, *19*, 297.
(8) Chattoraj, M.; King, B. A.; Bublitz, G. U.; Boxer, S. G. *Proc. Natl. Acad. Sci. U.S.A.* **1996**, *93*, 8362.
(9) Brejc, K.; Sixma, T. K.; Kitts, P. A.; Kain, S. R.; Tsien, R. Y.; Ormo, M.; Remington, S. J. *Proc. Natl. Acad. Sci. U.S.A.* **1997**, *94*, 2306.
(10) Palm, G. J.; Zdanov, A.; Gaitanaris, G. A.; Stauber, R.; Pavlakis, G. N.; Wlodawer, A. *Nat. Struct. Biol.* **1997**, *4*, 361.
(11) Lossau, H.; Kummer, A.; Heinecke, R.; Pollinger-Dammer, F.; Kompa, C.; Bieser, G.; Jonsson, T.; Silva, C. M.; Yang, M. M.; Youvan, D. C.; Michel-Beyerle, M. E. *Chem. Phys.* **1996**, *213*, 1.
(12) Creemers, T. M. H.; Lock, A. J.; Subramaniam, V.; Jovin, T. M.; Volker, S. *Nat. Struct. Biol.* **1999**, *6*, 557.
(13) Litvinenko, K. L.; Webber, N. M.; Meech, S. R. *Chem. Phys. Lett.* **2001**, *346*, 47.
(14) Litvinenko, K. L.; Webber, N. M.; Meech, S. R. *J. Phys. Chem. A* **2003**, *107*, 2616.
(15) Webber, N. M.; Litvinenko, K. L.; Meech, S. R. *J. Phys. Chem. B* **2001**, *105*, 8036.
(16) Niwa, H.; Inouye, S.; Hirano, T.; Matsuno, T.; Kojima, S.; Kubota, M.; Ohashi, M.; Tsuji, F. I. *Proc. Natl. Acad. Sci. U.S.A.* **1996**, *93*, 13617.

(17) Mandal, D.; Tahara, T.; Webber, N. M.; Meech, S. R. *Chem. Phys. Lett.* **2002**, *358*, 495.
(18) Klessinger, M.; Michl, J. *Excited States and Photochemistry of Organic Molecules*; VCH: Weinheim, Germany, 1995.
(19) Litvinenko, K. L.; Webber, N. M.; Meech, S. R. *Bull. Chem. Soc. Jpn.* **2002**, *75*, 1065.
(20) Follenius-Wund, A.; Bourotte, M.; Schmidt, M.; Lyice, F.; Lami, H.; Bourguignon, J.-J.; Haiech, J.; Pigault, C. *Biophys. J.* **2003**, *85*, 1839.
(21) Kummer, A. D.; Kompa, C.; Niwa, H.; Hirano, T.; Kojima, S.; Michel-Beyerle, M. E. *J. Phys. Chem. B* **2002**, *106*, 7554.
(22) Didier, P.; Guidoni, L.; Schwalbach, G.; Bourotte, M.; Follenius-Wund, A.; Pigault, C.; Bigot, J. Y. *Chem. Phys. Lett.* **2002**, *364*, 503.
(23) Liu, R. S. H.; Hammond, G. S. *Proc. Natl. Acad. Sci. U.S.A.* **2000**, *97*, 11153.
(24) Liu, R. S. H. *Acc. Chem. Res.* **2001**, *34*, 555.
(25) Weber, W.; Helms, V.; McCammon, J. A.; Langhoff, P. W. *Proc. Natl. Acad. Sci. U.S.A.* **1999**, *96*, 6177.
(26) Kennis, J. T. M.; Larsen, D. S.; van Stokkum, I. H. M.; Vengris, M.; van Thor, J. J.; van Grondelle, R. submitted.
(27) Larsen, D. S.; Vengris, M.; van Stokkum, I. H. M.; van der Horst, M.; Cordfunke, R.; Hellingwerf, K.; van Grondelle, R. In preparation.
(28) Larsen, D. S.; van Stokkum, I. H. M.; Vengris, M.; van der Horst, M.; Hellingwerf, K.; van Grondelle, R. submitted.
(29) Gai, F.; McDonald, J. C.; Anfinrud, P. *J. Am. Chem. Soc.* **1997**, *119*, 6201.
(30) Bell, A. F.; He, X.; Wachter, R. M.; Tonge, P. J. *Biochemistry* **2000**, *39*, 4423.
(31) Schellenberg, P.; Johnson, E.; Esposito, A. P.; Reid, P. J.; Parson, W. W. *J. Phys. Chem. B* **2001**, *105*, 5316.
(32) Gradinaru, C. C.; van Stokkum, I. H. M.; Pascal, A. A.; van Grondelle, R.; van Amerongen, H. *J. Phys. Chem. B* **2000**, *104*, 9330.
(33) Larsen, D. S.; Vengris, M.; van Stokkum, I. H. M.; van der Horst, M.; de Weerd, F. L.; Hellingwerf, K. J.; van Grondelle, R. *Biophys. J.* **2004**, *86*, 2538.
(34) van Stokkum, I. H. M.; Scherer, T.; Brouwer, A. M.; Verhoeven, J. W. *J. Phys. Chem.* **1994**, *92*, 852
(35) Holzwarth, A. R. Data Analysis in time-resolved measurements. In *Biophysical Techniques in Photosynthesis*; Amesz, J., Hoff, A. J., Eds.; Kluwer: Dordrecht, The Netherlands, 1996.
(36) de Weerd, F. L.; van Stokkum, I. H. M.; van Grondelle, R. *Chem. Phys. Lett.* **2002**, *354*, 38.
(37) van Stokkum, I. H. M.; Larsen, D. S.; van Grondelle, R. submitted.
(38) Muller, M. G.; Drews, G.; Holzwarth, A. *Chem. Phys. Lett.* **1996**, *258*, 194.
(39) Zhang, J. P.; Inaba, T.; Watanabe, Y.; Koyama, Y. *Chem. Phys. Lett.* **2001**, *340*, 484.
(40) Papagiannakis, E.; Kennis, J. T. M.; van Stokkum, I. H. M.; Cogdell, R. J.; van Grondelle, R. *Proc. Natl. Acad. Sci. U.S.A.* **2002**, *99*, 6017.
(41) Larsen, D. S.; Papagiannakis, E.; van Stokkum, I. H. M.; Vengris, M.; Kennis, J. T. M.; van Grondelle, R. *Chem. Phys. Lett.* **2003**, *381*, 733.
(42) He, X.; Bell, A. F.; Tonge, P. J. *FEBS Lett.* **2003**, *549*, 35.
(43) Ruhman, S.; Hou, B.; Freidman, N.; Ottolenghi, M.; Sheves, M. *J. Am. Chem. Soc.* **2002**, *124*, 8854.
(44) Vilchiz, V. H.; Kloepfer, J. A.; Germaine, A. C.; Lenchenkov, V. A.; Bradforth, S. E. *J. Phys. Chem. A* **2001**, *105*, 1711.
(45) Long, F. H.; Lu, H.; Eisenthal, K. B. *Phys. Rev. Lett.* **1990**, *64*, 1469.
(46) Jou, F.-Y.; Freeman, G. R. *J. Phys. Chem.* **1979**, *83*, 2383.
(47) Changenet-Barret, P.; Espagne, A.; Katsonis, N.; Charier, S.; Baudin, J.-B.; Jullien, L.; Plaza, P.; Martin, M. M. *Chem. Phys. Lett.* **2002**, *365*, 285.
(48) Changenet-Barret, P.; Plaza, P.; Martin, M. M. *Chem. Phys. Lett.* **2001**, *336*, 439.
(49) Martin, M. M.; Plaza, P.; Changenet-Barret, P.; Siemiarczuk, A. *J. Phys. Chem. A* **2002**, *106*, 2351.
(50) Larsen, D. S.; Vengris, M.; van Stokkum, I. H. M.; van der Horst, M.; Cordfunke, R.; Hellingwerf, K. J.; van Grondelle, R. *Chem. Phys. Lett.* **2003**, *369*, 563.
(51) Lachish, U.; Shafferman, A.; Stein, G. *J. Chem. Phys.* **1975**, *64*, 4205.
(52) Gauduel, Y.; Pommeret, S.; Migus, A.; Antonetti, A. *J. Phys. Chem.* **1989**, *93*, 3880.
(53) Lu, H.; Long, F. H.; Bowman, R. M.; Eisenthal, K. B. *J. Phys. Chem.* **1989**, *93*, 27.
(54) Goulet, T.; Jaygerin, J. P. *J. Chem. Phys.* **1992**, *96*, 5076.
(55) Buxton, G. V.; Greenstock, C. L.; Helman, W. P.; Ross, A. B. *J. Phys. Chem. Ref. Data* **1988**, *17*, 513.
(56) Winkler, K.; Lindner, J. R.; Subramaniam, V.; Jovin, T. M.; Vohringer, P. *Phys. Chem. Chem. Phys.* **2002**, *4*, 1072.
(57) Abramavicius, D.; Gulbinas, V.; Valkunas, L.; Shiu, Y.-J.; Liang, K.; Hayashi, M.; Lin, S. *J. Phys. Chem. A* **2002**, *106*, 8864.
(58) Hamm, P.; Zurek, M.; Röschinger, T.; Patselt, H.; Oesterhelt, D.; Zinth, W. *Chem. Phys. Lett.* **1996**, *263*, 613.
(59) Fain, B. *Irreversibilities in quantum mechanics*; Kluwer Academic Publishers: Dordrecht, The Netherlands, 2000.
(60) Toniolo, A.; Ben-Nun, M.; Martínez, T. J. *J. Phys. Chem. A* **2002**, *106*, 4679.
(61) Toniolo, A.; Granucci, G.; Martínez, T. J. *J. Phys. Chem. A* **2003**, *107*, 3822.
(62) Maroncelli, M. *J. Mol. Liq.* **1993**, *57*, 1.
(63) Jimenez, R.; Fleming, G. R.; Kumar, P. V.; Maroncelli, M. *Nature* **1994**, *369*, 471.
(64) Kovalenko, S. A.; Ernsting, N. P.; Ruthmann, J. *J. Chem. Phys.* **1997**, *106*, 3504.
(65) Kovalenko, S. A.; Ruthmann, J.; Ernsting, N. P. *Chem. Phys. Lett.* **1997**, *271*, 40.
(66) Kovalenko, S. A.; Ruthmann, J.; Ernsting, N. P. *J. Chem. Phys.* **1998**, *109*, 1894.
(67) Changenet-Barret, P.; Choma, C.; Gooding, E.; DeGrado, W.; Hochstrasser, R. M. *J. Phys. Chem. B* **2000**, *104*, 9322.
(68) Dobler, J.; Zinth, W.; Kaiser, W.; Oesterhelt, D. *Chem. Phys. Lett.* **1988**, *144*, 215.
(69) Stratt, R. M.; Maroncelli, M. *J. Phys. Chem.* **1996**, *100*, 12981.
(70) Horng, M. L.; Gardecki, J. A.; Papazyan, A.; Maroncelli, M. *J. Phys. Chem.* **1995**, *99*, 17311.
(71) Oster, G.; Nishijima, Y. *J. Am. Chem. Soc.* **1956**, *78*, 1581.
(72) Migus, A.; Gauduel, Y.; Martin, L. J.; Antonetti, A. *Phys. Rev. Lett.* **1987**, *58*, 1559.
(73) Jordanides, X. J.; Lang, M. J.; Song, X. Y.; Fleming, G. R. *J. Phys. Chem. B* **1999**, *103*, 7995.
(74) Toniolo, A.; Olsen, S.; Manohar, L.; Martínez, T. J. *Faraday Discuss.* **2004**, in press.
(75) Mandal, D.; Tahara, T.; Meech, S. R. in press.
(76) Gardecki, J.; Horng, M. L.; Papazyan, A.; Maroncelli, M. *J. Mol. Liq.* **1995**, *65*−*6*, 49.
(77) Rosenthal, S. J.; Jimenez, R.; Fleming, G. R.; Kumar, P. V.; Maroncelli, M. *J. Mol. Liq.* **1994**, *60*, 25.
(78) Lang, M. J.; Jordanides, X. J.; Song, X.; Fleming, G. R. *J. Chem. Phys.* **1999**, *110*, 5884.
(79) Vengris, M.; Larsen, D. S.; Chergui, M.; van Stokkum, I. H. M.; Haacke, S.; van Grondelle, R. in preparation.
(80) Chosrowjan, H.; Mataga, N.; Shibata, Y.; Imamoto, Y.; Tokunaga, F. *J. Phys. Chem. B* **1998**, *102*, 7695.
(81) Das, A. K.; Hasegawa, J. Y.; Miyahara, T.; Ehara, M.; Nakatsuji, H. *J. Comput. Chem.* **2003**, *24*, 1421.
(82) Bublitz, G.; King, B. A.; Boxer, S. G. *J. Am. Chem. Soc.* **1998**, *120*, 9370.
(83) Fonseca, T.; Ladanyi, B. M. *J. Phys. Chem.* **1991**, *95*, 2116.
(84) Kovalenko, S. A.; Schanz, R.; Hennig, H.; Ernsting, N. P. *J. Chem. Phys.* **2001**, *115*, 3256.
(85) Nikowa, L.; Schwarzer, D.; Troe, J. *Chem. Phys. Lett.* **1995**, *233*, 303.
(86) Groenhof, G.; Lensink, M. F.; Berendsen, H. J. C.; Mark, A. E. *Proteins: Struct., Funct., Genet.* **2002**, *48*, 212.
(87) Groenhof, G.; Lensink, M. F.; Berendsen, H. J. C.; Snijders, J. G.; Mark, A. E. *Proteins: Struct., Funct., Genet.* **2002**, *48*, 202.
(88) Toniolo, A.; Olsen, S.; Manohar, L.; Martínez, T. J. *Faraday Discuss.*, in press.
(89) Waldeck, D. H. *Chem. Rev.* **1991**, *91*, 415.
(90) Ko, C.; Levine, B.; Toniolo, A.; Monohar, L.; Olsen, S.; Werner, H.-J.; Martínez, T. J. *J. Am. Chem. Soc.* **2003**, in press.
(91) Hasson, K. C.; Gai, F.; Anfinrud, P. A. *Proc. Natl. Acad. Sci. U.S.A.* **1996**, *93*, 15124.
(92) Humphrey, W.; Lu, H.; Logunov, I.; Werner, H. J.; Schulten, K. *Biophys. J.* **1998**, *75*, 1689.
(93) Gai, F.; Hasson, K. C.; McDonald, J. C.; Anfinrud, P. A. *Science* **1998**, *279*, 1886.
(94) Sanchez-Galvez, A.; Hunt, P.; Robb, M. A.; Olivucci, M.; Vreven, T.; Schlegel, H. B. *J. Am. Chem. Soc.* **2000**, *122*, 2911.
(95) Ryan, W.; Gordon, D. J.; Levy, D. H. *J. Am. Chem. Soc.* **2002**, *124*, 6194.
(96) Voityuk, A. A.; Michel-Beyerle, M. E.; Rosch, N. *Chem. Phys. Lett.* **1998**, *296*, 269.
(97) Toniolo, A.; Olsen, S.; Manohar, L.; Martínez, T. J. *Ultrafast excited-state dynamics in the green fluorescent protein chromophore*; Femtosecond V, Paris, 2003.
(98) Groenhof, G.; Bouxin-Cademartory, M.; Hess, B.; de Visser, S.; Brendendsen, H.; Olivucci, M.; Mark, A. E.; Robb, M. A. *J. Am. Chem. Soc.* **2004**, *126*, 4228.